J Petrol Explor Prod Technol (2016) 6:117–127
DOI 10.1007/s13202-015-0173-y

ORIGINAL PAPER - PRODUCTION ENGINEERING

Pumping crude oil by centrifugal impeller having different blade angles and surface roughness

Sayed Ahmed Imran Bellary[1] · **Abdus Samad**[1]

Received: 19 January 2015 / Accepted: 17 May 2015 / Published online: 9 June 2015

Abstract Centrifugal pumps are extensively used in the oil and gas industries and the pump performance drops with higher viscosity and higher surface roughness of the pump impeller, and the impeller design parameters have significant effect on the pump performance. Through the present research, crude oil pumping behavior has been predicted, analyzed and compared with other fluids. A 3D flow simulation using Reynolds-averaged Navier–Stokes (RANS) equation was performed by considering different blade angles and impeller surface roughness to pump crude oil, kerosene, gasoline, saline-water and water. Standard k-ε two-equation turbulence model was used for the turbulent closure of steady incompressible flow. The investigation shows that the blade angles have significant influence on the head, input power and efficiency of the impeller for different liquids. Higher head and power, and lower hydraulic efficiency were observed with higher surface roughness values.

Keywords Centrifugal impeller · Exit blade angle · Viscosity · Roughness · Slip factor

✉ Abdus Samad
samad@iitm.ac.in

Sayed Ahmed Imran Bellary
ibellary@gmail.com

[1] Wave Energy and Fluids Engineering Laboratory, Department of Ocean Engineering, Indian Institute of Technology Madras, Chennai 600036, India

List of symbols

Abbreviations

RANS	Reynolds-averaged Navier–Stokes
CFD	Computational fluid dynamics
PS	Pressure side
SS	Suction side
LE	Leading edge
TE	Trailing edge

Description

B	Blade width (mm)
C	Absolute fluid flow velocity (m/s)
c_{eq}	Equivalence factor
c_m	Meridional velocity component (m/s)
c_u	Peripheral velocity component (m/s)
D	Diameter (m)
f	Fluid
f_i	Body force (N)
f_R	Roughness effect
g	Acceleration due to gravity (m/s^2)
H	Head generated (m)
ΔH	Hydraulic losses (m)
k_s	Sand roughness (μm)
k_s^+	Roughness Reynolds number
m	Mass flow rate (kg/s)
N	Impeller speed (rpm)
P	Power consumed by pump (kW)
p	Pressure (N/m^2)
Q	Volume flow rate (m^3/s)
Re	Reynolds number
r	Radius (m)
t	Total blade thickness (mm)
U_j	Three-dimensional velocity vector
U	Peripheral velocity (m/s)
u_τ	Frictional velocity (m/s)

w Relative fluid velocity (m/s)
w_u Peripheral component of w (m/s)
w_s Relative velocity on suction side (m/s)
y Blade thickness
z Blade number

Greek symbol

β Blade angle (°)
ε Rate of kinetic energy dissipation (J/s)
η Hydraulic efficiency (%)
k Turbulence kinetic energy (J)
μ Dynamic viscosity (N s/m^2)
v Kinematic viscosity (m^2/s)
ρ Density of fluid (kg/m^3)
σ Slip factor
τ_{ij} Viscous stress tensor
τ_w Shear stress at the wall (N/m^2)

Subscript

1 Inlet
2 Outlet
a Actual
h Hub
o Eye
s Shaft
th Theoretical
max Maximum

Introduction

Now-a-days centrifugal pump either as single stage or multistage is extensively used in upstream, midstream and downstream oil industries. For example, the upstream oil industry uses to lift fluid from the wellbore, to deliver fluid in the separation system, etc. Performance characteristics of a pump greatly depend on geometry and surface property of an impeller. Again, the viscosity which can be defined as resistance to flow has significant impact on head, efficiency and power consumption of the pump.

Many researchers reported analysis of centrifugal pump for the flow behavior, influence of geometric parameters, etc. (Kamimoto and Matsuoka 1956; Varley 1961; Stepanoff 1940; Lazarkiewicz and Troskolanski 1965). The works on inlet and exit blade angle shows that the performance can be altered, when the angles are modified. A higher exit blade angle was suggested by the researchers. Kamimoto and Matsuoka (1956) experimentally investigated the effect of exit blade angles and reported that the impeller with 30° exit angle has the best performance. For a double suction centrifugal pump, the head increment can be achieved by increasing exit blade angle and an improvement in efficiency by varying exit blade angles can be obtained (Varley 1961). The inlet blade angle modification of a radial impeller has been reported by Sanda and Daniela (2012), and Luo et al. (2008). They reported that performance enhancement is possible by this modification.

Normally, pump designers design the pumps for water and they rarely test for different viscosities. Obviously, higher viscosity has detrimental effect on performance as the higher viscosity has more resistance to flow (Murakami et al. 1980; Telow 1942; Ippen 1946; Itaya and Nishikawa 1960). Again, the density effect has not been considered by the researchers. If the fluid is having higher viscosity or density it is inevitable to check amount of extra power consumption required and this will help energy auditing of a company. The power requirement of pump selection on the basis of the head requirement can be evaluated. Reports on centrifugal pump handling viscosity liquids shows that that the large exit angle exhibits an improvement in head and efficiency (Aoki et al. 1947; Ohta and Aoki 1996; Fard and Boyaghchi 2007). Li (2011) investigated the effect of various blade angles of an industrial oil and concluded that the blade exit angle has equal effects on head, power and efficiency. Shojaeefard et al. (2012) investigated both experimentally and numerically the effect of impeller exit angle for oil as working fluid and showed that increase of impeller outlet angle leads to improvement in the performance. Shigemitsu et al. (2011) performed experiment and numerical analysis on a mini turbo-pump and reported that the flow rate of the maximum efficiency shifts to a large flow rate due to the increase of the blade exit angle.

If any centrifugal pump works for a longer period, the surface gets deteriorated because of fouling, cavitation or erosion. The oil industry typically handles multi-phase flow and the phases are oil, water gas and sand. There may be some corrosive gasses also such as H_2S. The acidic gas H_2S reacts with water and forms H_2SO_4 which is highly reactive to the metal. Similarly CO_2 or Cl gives ion for corrosion of metal. These corrosive gasses along with sand-jetting effect accelerate the erosion. A small amount of sand can initiate pitting on the surface and the new surface is attacked by the reactive gasses or acids. Hence, the pump handling fluid from the well bore or at the surface production operations or at the downstream petroleum processing industries will develop micro-pitting and as a result there will be surface roughness. On one side the oil or the liquid hydrocarbon (HC) coats the surface and helps reducing the reaction, but at the same time it resists the flow through the pump. The high-density fluid can have higher head but the pump may be running under off-design condition. Hence, finally pump performance will be dropped.

Experiments for different surface roughness values were conducted by Varley (1961), but they did not report the inter-dependency of exit blade angle with surface

roughness. Fard and Boyaghchi (2007) studied the influence of various blade exit angles to handle viscous fluids by computational and experimental methods. The investigation did not include roughness of wet wall. Li (2011) reported effect of exit blade angle, viscosity and roughness by CFD simulations, but the effect of inlet and outlet blade angle on roughness was not included.

Several researchers (Johnston and Rothe 1967; Johnston et al. 1972; Bayly and Orszag 1988) reported a low-energy separated region, i.e., a boundary layer on pressure side which is unstable and tends to propagate from the hub and shroud surfaces on the suction side in the impeller. This kind of flow pattern develops jet wake flow. The analytical and experimental results (Dean and Senoo 1960; Tuzson 1993) show that a separated region because of acceleration and corresponding pressure increase from suction side to pressure side forming a separated region has its limitations. This kind of jet wake flow pattern is exhibited only under certain conditions.

Thus, the purpose of the present study is to investigate the combined effect of blade angles and surface roughness on impeller performance by numerical simulation for crude oil, kerosene, gasoline, saline-water, and water at different flow rates. The flow mechanism, nature and distribution of velocity and pressure in the pump at design and off-design point were reported. Reason to find performance change due to viscosity effect in a centrifugal pump was performed at different conditions.

Numerical formulation

In the present problem, a centrifugal pump impeller was considered (Fig. 1; Table 1). The detail geometry of the impeller corresponds to the values obtained from the conventional design procedure of impeller design as given in refs. (Lazarkiewicz and Troskolanski 1965; Stepanoff 1964; Church 1972). The same geometry has already been reported by the authors (Bellary et al. 2014; Bellary and Samad 2014). Design procedures (Lazarkiewicz and Troskolanski 1965; Church 1972) and the input values such as head (H), discharge (Q), and impeller speed (N) were considered for the same reference. The blades had constant thickness (y) and width (b) with trailing edge chamfered.

To investigate the influence of blade angles on the performance of centrifugal impeller, three inlet blade angles ($\beta_1 = 17°$, 23° and 28°) and three outlet blade angles ($\beta_2 = 25°$, 40° and 70°) were considered. Surface roughness was changed from hydrodynamically smooth surface to a sand roughness of 50 and 100 µm. Here, hydrodynamically smooth surface refers to a roughness of 5 µm. Table 2 represents the liquids used for the analyses. All the simulations were performed at 20 °C temperature.

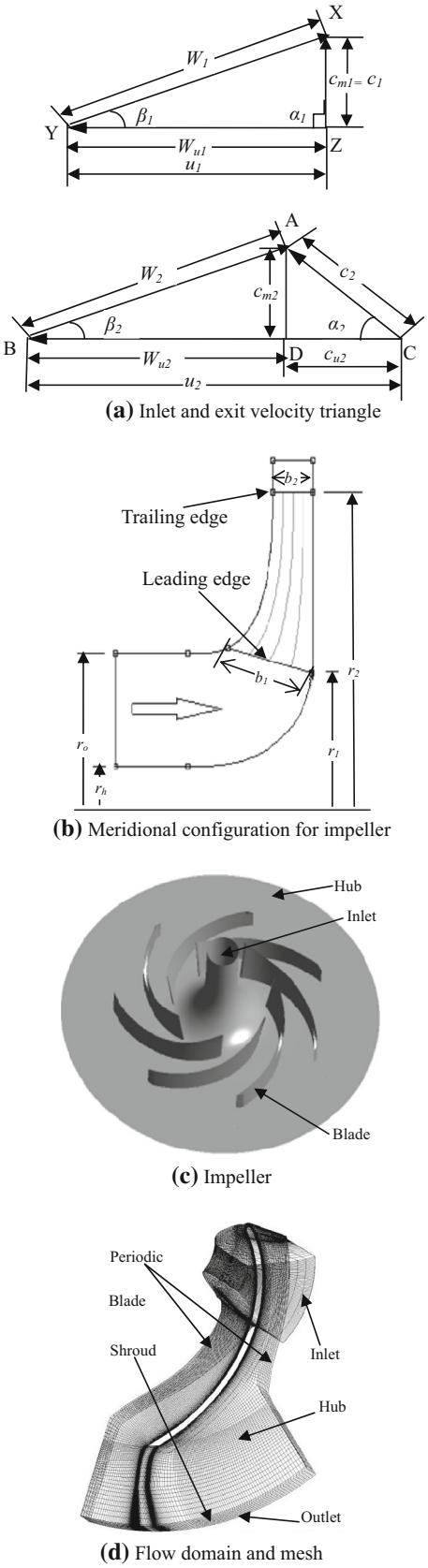

Fig. 1 Computational domain

Table 1 Features of impeller

Parameter	Dimension
Shaft diameter, D_s	40 mm
Eye diameter, D_o	182 mm
Hub diameter, D_h	55 mm
Inlet diameter, D_1	160 mm
Inlet blade width, b_1	54 mm
Outlet blade width, b_2	30 mm
Inlet blade angle, β_1	17°, 23° and 28°
Outlet blade angle, β_2	25°, 40° and 70°
Blade number, z	7
Outlet diameter, D_2	365 mm

Table 2 Viscosity and density of different fluids

Fluid	Viscosity (N s/m^2)	Density (kg/m^3)
Water	1.002E-3	997
Saline-water	1.080E-3	1031
Crude oil	5.000E-3	835
Gasoline	5.000E-4	720
Kerosene	2.100E-3	810

Table 3 Meshing and boundary conditions

Parameter	Description
Flow domain	Single impeller
Interface	Periodic
Mesh/nature	Structural/hexahedral
Nodes	634,161
Elements	568,620
Fluid nature	Water, saline-water, crude oil, gasoline and kerosene
Inlet	Pressure
Outlet	Mass flow rate
Residual convergence value	1×10^{-5}
Time taken for simulation	15 h
Iteration steps	2000
Mass imbalance	0.0001 %

CAD modeling and meshing of the flow domain were carried out by using Ansys-BladeGen and -TurboGrid module, respectively (Ansys-CFX 13.0 2010). Ansys-CFX 13.0 (2010) was used for the flow simulations. The total number of nodes, elements, convergence criteria and iteration steps, etc., are given in Table 3. The mesh in the flow passage was with O-grid block, and it was with H-grid block at the inlet and outlet. To achieve linear velocity distribution in the viscous sublayer, higher number of cells

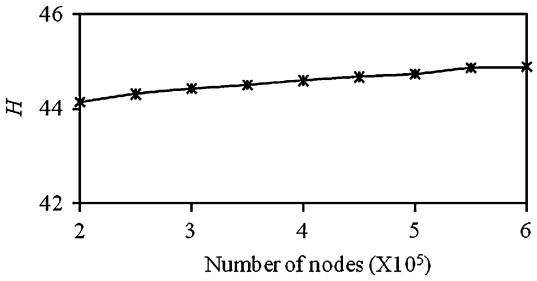

Fig. 2 Head variation with number of nodes at design flow rate ($Q = 0.1003$ m^3/s)

was employed near the wall. To avoid fine mesh inconsistencies and to resolve the boundary layer, at least 10 nodes were included into the boundary layer (Ansys-CFX 13.0 2010; Gulich 2010). In all simulations performed the size of elements used next to wall was 11.13. Figure 2 shows head variation with the number of nodes of the flow domain.

The Reynolds-averaged Navier–Stokes (RANS) equations for steady, incompressible turbulent flow of constant properties fluids can be written in tensor form as:

$$\frac{\partial U_i}{\partial x_i} = 0 \tag{1}$$

$$\rho_f U_j \frac{\partial U_i}{\partial x_j} = -\frac{\partial P}{\partial x_i} + \frac{\partial}{\partial x_j}\left[(\mu_f + \mu_t)\left(\frac{\partial^2 U_i}{\partial x_j \partial x_j}\right)\right] \tag{2}$$

Here, turbulent viscosity is modeled by the k-ε model (turbulence model) as:

$$\mu_t = C_\mu \rho_f \frac{k^2}{\varepsilon} \tag{3}$$

The equations for turbulent kinetic energy and dissipation rate can be written as:

$$\rho_f U_j \frac{\partial k}{\partial x_j} = \frac{\partial}{\partial x_j}\left[\left(\mu_f + \frac{\mu_t}{\sigma_k}\right)\frac{\partial k}{\partial x_j}\right] + P_k - \rho_f \varepsilon \tag{4}$$

$$\rho_f U_j \frac{\partial \varepsilon}{\partial x_j} = \frac{\partial}{\partial x_j}\left[\left(\mu_f + \frac{\mu_t}{\sigma_\varepsilon}\right)\frac{\partial \varepsilon}{\partial x_j}\right] + \frac{\varepsilon}{k}(C_{\varepsilon 1} P_k - C_{\varepsilon 2}\rho_f \varepsilon), \tag{5}$$

where

$$P_k = \mu_t\left(\frac{\partial U_i}{\partial x_j} + \frac{\partial U_j}{\partial x_i}\right)\frac{\partial U_i}{\partial x_j} \tag{6}$$

The values of the closing constants are $C_\mu = 0.09$, $C_{\varepsilon 1=}1.44$, $C_{\varepsilon 2} = 1.92$, $\sigma_k = 1.0$, and $\sigma_\varepsilon = 1.3$.

To account for Reynolds number (Re $> 10^5$), the standard k-ε turbulence model was employed. Within Ansys-CFX (2010), the k-ε turbulence model uses the scalable wall-function approach to improve robustness and accuracy. High-resolution upwind discretization scheme was

used for solving convection terms with central difference schemes for diffusion terms. Ansys-CFX (2010) solver is a coupled solver and solves the hydrodynamic equations for velocity and pressure (u, v, w, p) as a single system. The simulations were carried out on 3.4 GHz core i7-3370 processor with 8 GB ram. Time per iteration was within 21 s.

Backward swept ($\beta_2 < 90^o$) blades are used in pumps and blowers (Srinivasan 2008). The blade angles have influence on the total head and efficiency of pump. As per Euler's equation, head generated by an impeller blade is given by

$$H = \frac{c_{u2}u_2 - c_{u1}u_1}{g}. \tag{7}$$

Normal entry at impeller inlet implies $c_{u1} = 0$ and from velocity triangle shown in Fig. 1a c_{u2} can be given as:

$$c_{u2} = u_2 - \frac{Q\cot\beta_2}{\pi D b_2}. \tag{8}$$

From Fig. 1a it is clear that as β_2 increases, the absolute exit velocity c_2 also increases. Increase in c_2 causes c_{u2} to increase which results in increase in head.

Slip factor (σ) generally explains the slip effect at the impeller exit and the factor is used to specify theoretical head developed by an impeller (Srinivasan 2008). The slip factor is estimated by the relation,

$$\sigma = 1 - \frac{\pi\sin\beta_2}{z}. \tag{9}$$

Input power in terms of c_{u2} is given by

$$P = \frac{\rho g Q u_2 c_{u2}}{g}. \tag{10}$$

The Eqs. (8) and (10) indicate that the increase in exit angle results in increase in c_{u2} which increases the input power.

Hydraulic efficiency is given by

$$\eta = \frac{H_a}{H_{th}} = \frac{H_{th} - \Delta H}{H_{th}}. \tag{11}$$

The hydraulic losses and theoretical head (H_{th}) at design point differ from the off-design conditions. The head and the corresponding efficiency are higher for a larger exit angle (Srinivasan 2008).

Surface roughness

Surface roughness increases the flow resistance in turbulent flow. It has no effect on the resistance due to no exchange of momentum across the flow in laminar flow condition. A wall is termed as hydraulically smooth if all the roughness peaks are within the laminar sublayer. Increase in Reynolds number (R_e) results in decrease in boundary layer thickness. A hydraulically rough surface has some peaks greater than the boundary layer thickness. Surface roughness is expressed in term sand roughness (k_s). The sand roughness considers a uniform surface structure while the surfaces may have irregular roughness which considers maximum roughness depth k_{smax} (Gulich 2010; Tuzson 2000) in actual scenario. The relationship between k_s and k_{smax} is given by

$$c_{eq} = \frac{k_{smax}}{k_s}. \tag{12}$$

As per Tuszon (2000), the roughness Reynolds number k_s^+ can be defined as the ratio of frictional force to the viscous force, and given by

$$k_s^+ = \frac{u_\tau k_s}{v} \tag{13}$$

$$u_\tau = \sqrt{\frac{\tau_w}{\rho}}. \tag{14}$$

Disc friction losses become significant for higher k_s and the hydraulic losses as well as efficiency get increased (Eq. 11). Energy losses in impeller depend on Reynolds number and relative surface roughness and termed as roughness effect (Gulich 2010). The roughness effect (f_R) on disc friction can be given as:

$$f_R = \left\{\frac{\log\frac{12.5}{R_e}}{\log\left(0.2\frac{k_s}{r_2} + \frac{12.5}{R_e}\right)}\right\}^{2.15}. \tag{15}$$

Results and discussion

Problem setup

Initially, the pump geometry was designed and grid-dependency test (Fig. 2), check for turbulence model and validity of the CFD simulations were checked for water at design flow condition. The number of nodes was 550,000 for all the simulations as the variation of head with the increase in number of nodes were not significant. Further it was checked for accuracy of the CFD model and found that the results were predicting well (Bellary et al. 2014; Bellary and Samad 2014). After that the geometry was changed for different inlet and exit angles, and different surface roughness. The simulations were done for different fluids and for a wider operating range.

Effect of blade angles

The simulations were carried out at different mass flow rates and initially parametric study was performed for different

inlet and exit angles ($\beta_1 = 17°–28°$ and $\beta_2 = 25°–70°$). Figure 4 represents the performance curves for different combinations of the inlet and exit angles. The impeller with $\beta_1 = 23°$ has slightly better performance as compared to $\beta_1 = 17°$ and $28°$ designs, hence all further calculations were performed at $\beta_1 = 23°$ with different β_2. Figure 5 demonstrates the head, shaft power and hydraulic efficiency at different flow rates. Large β_2 results in an increase in head. This is due to the increase in absolute flow velocity at exit (c_2) and the corresponding peripheral velocity (c_{u2}), i.e., dynamic part of the head increases more rapidly.

From Eq. (7) it is obvious that the head increases with the increase in c_{u2}. Equation (8) represents a drooping down straight line and says that a larger discharge angle produces a higher head than a smaller exit angle. The maximum change of the head curve due to the variation in discharge angle is almost same for the fluids. This implies that the effect of discharge angle on the head curve is independent of the fluid viscosity ($\mu = 5.0\text{E} - 4$ to $50.0\text{E} - 4$ N-s/m^2). Irrespective of viscosity, the maximum change in head due to the change in β_2 remains almost same (Fig. 5). Thus, effect of discharge angle on head is independent of the viscosity of fluid being used.

For the same flow rate and discharge angle, the input power is more for denser fluids (Fig. 5b) and this is explained by Eq. (10). The increase in flow rate results in increase in power consumption. The density of crude oil, gasoline or kerosene is lesser than that of water or saline-water, which causes the lesser power consumption. Higher β_2 increases c_{u2}; hence, the power consumption by the impeller is more (Eq. 10).

A large exit angle favors efficiency enhancement (Fig. 5). The efficiency is maximum at the best efficiency point and gets reduced uniformly to the right of the best efficiency point. At this point, secondary and profile losses are minimum and at the off-design points the secondary and shock losses increases which increases total hydraulic losses resulting in reduced efficiency (Srinivasan 2008). The efficiency for crude oil, saline-water, gasoline or kerosene is lower than that for water. The decrease in efficiency, while pumping the crude oil and saline-water is due to the disc friction losses over the outsides of the impeller shroud and hub due to viscous effect. The results agree with the results of Gulich (2010) and Li (2008).

Contours of static pressure and liquid flow velocity for design point ($Q = 0.1003$ m^3/s) at 50 % span are shown in Figs. 6 and 7. The static difference between impeller inlet and outlet increases with large β_2. This happens because of fluid flow velocity at impeller outlet, which decreases with increase in discharge angle. The contours depict a smooth flow and the pressure increases continuously towards the exit of the domain. The lowest static pressure can be observed at the impeller inlet on suction side (Fig. 6). At this

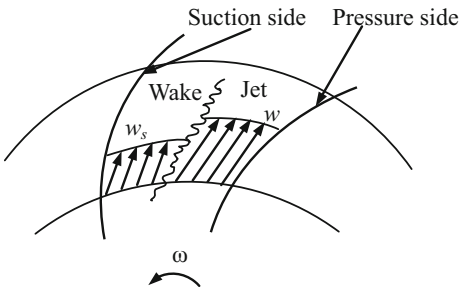

Fig. 3 Jet-wake flow pattern in impeller

location, usually an inception of cavitation appears. In the present work, the fluids were at the above saturation pressure and the occurrence of cavitation is ruled out (Gulich 2010).

The static pressure and kinetic energy reaches a peak value at the impeller exit. This is due to the energy transfer by the impeller to the fluid. Lowest pressure exists at the suction side (near the leading edge) of the impeller. With the increase in blade angle, the pressure difference between outlet and inlet increases. The liquids with large β_2 have higher pressure difference because of the decrease in velocity at the impeller outlet for large β_2 (Fig. 5). This agrees with the existing analytical results (Lazarkiewicz and Troskolanski 1965; Srinivasan 2008).

For a radial blade impeller jet wake flow pattern can be observed if $\sin(\beta)$ is relatively lesser than the ratio of the average velocity on the seperating streamline and circumferential velocity (Tuzson 2000). However, with backward curved vanes, the blades lean strongly backwards making $\sin(\beta)$ relatively large and the above statement does not hold good. Hence, jet wake flow pattern shown in Fig. 3 was not observed in the pumps (Tuzson 2000).

Effect of surface roughness

As stated earlier in this paper that the surface roughness helps dropping performance and it is supposed to have less performance if water is pumped. The following discussion tries to highlight its effect for different viscosity fluid and the design aspects of blade angles.

The properties the fluids (Table 2) were used to find the effect of roughness and viscosity for different exit blade angles on the pump performance. Characteristic curves for $Q = 0.1003$ m^3/s, $N = 1470$ rpm with $k_s = 0$, 50 and 100 μm have been shown in Fig. 8. Increase in surface roughness increases the head (H), input power (P) and decreases the efficiency (η) (Varley 1961; Li 2008). It is quite obvious that the pumping performance of the roughened hub and shrouds is increased. This results in an increase in head. A decrease in efficiency with higher k_s values can be noticed. This occurs due to the flow losses in the impeller passages and also due to external disc friction (Varley 1961).

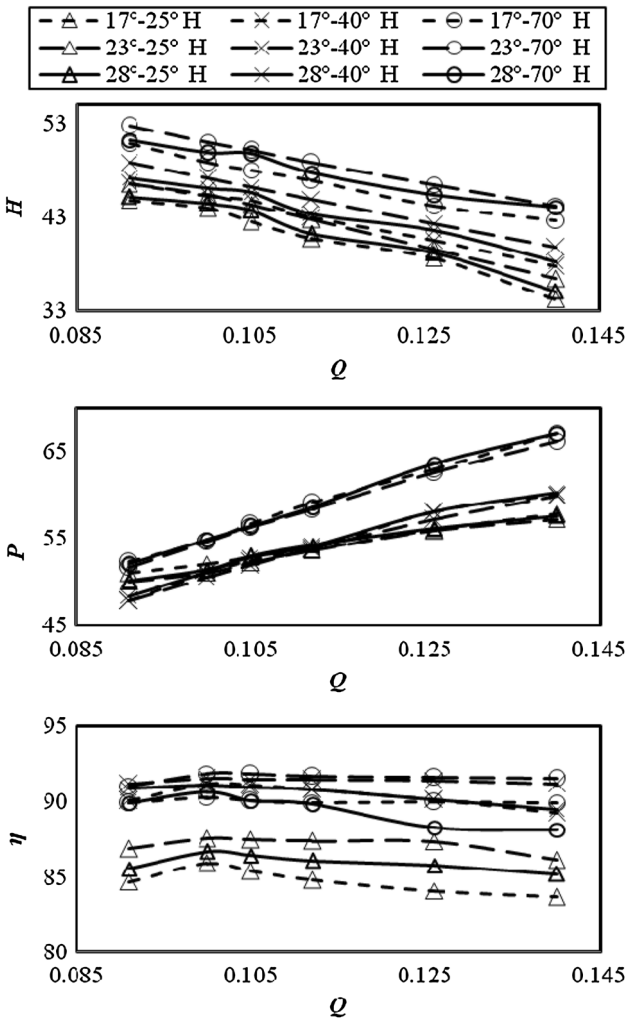

Fig. 4 Performance curves for water at different blade angles (The legend for each *line*/*symbol* shows that the first number is β_1 and the second number is β_2.)

Combined effect of exit blade angle and roughness

The results show that head generation increases due to the combined effect of increase in β_2 and k_s values. Rough surface implies a deceleration of relative velocity near the solid walls with boundary layer thickening (Fig. 9). A large β_2 results in an increase in slip factor (Eq. 9). An increase in slip factor and head is caused by the lower relative velocity. Also a roughness increase of the impeller passages result in a small increase in head; in such cases the roughness has an effect on the slip factor through an increase of the absolute velocity in the boundary layers and an impact on secondary flow. As the exit blade angle increases, the length of the blades decreases resulting into greater friction losses in the longer impeller passages. A large exit blade angle facilitates the fluid to leave the impeller with a high absolute velocity which is responsible for large mixing and great skin friction

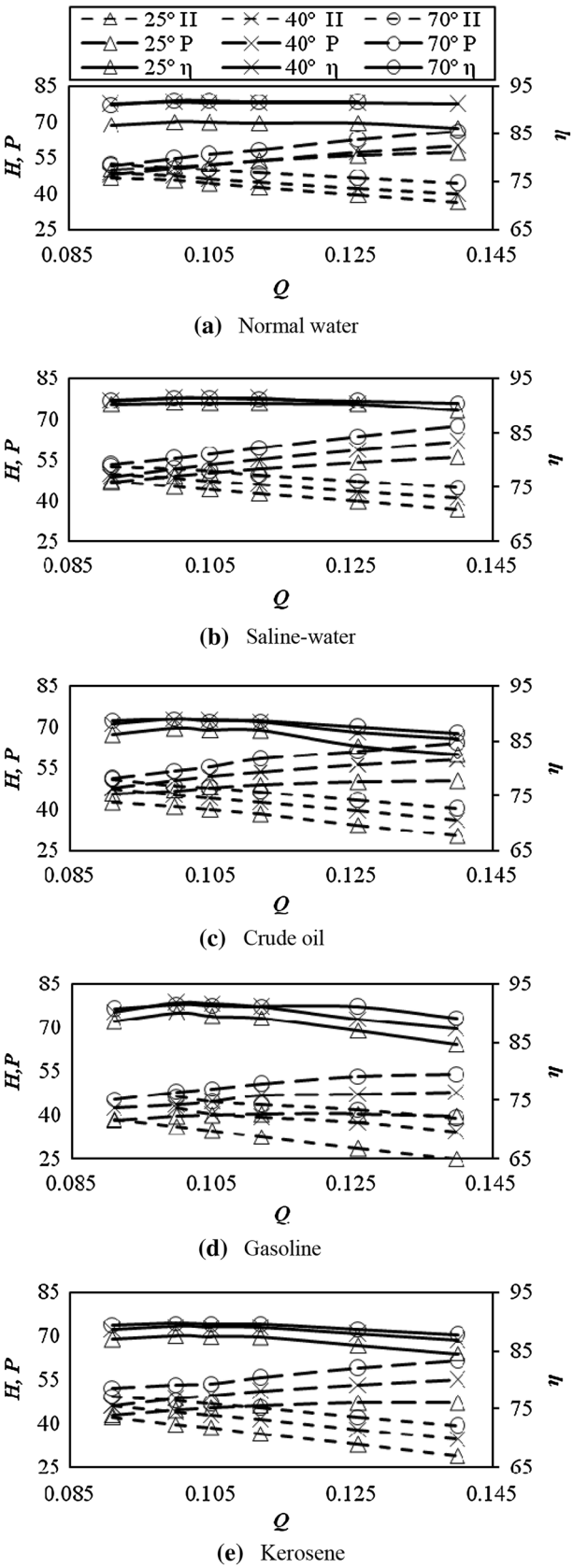

Fig. 5 Performance curves for different fluids

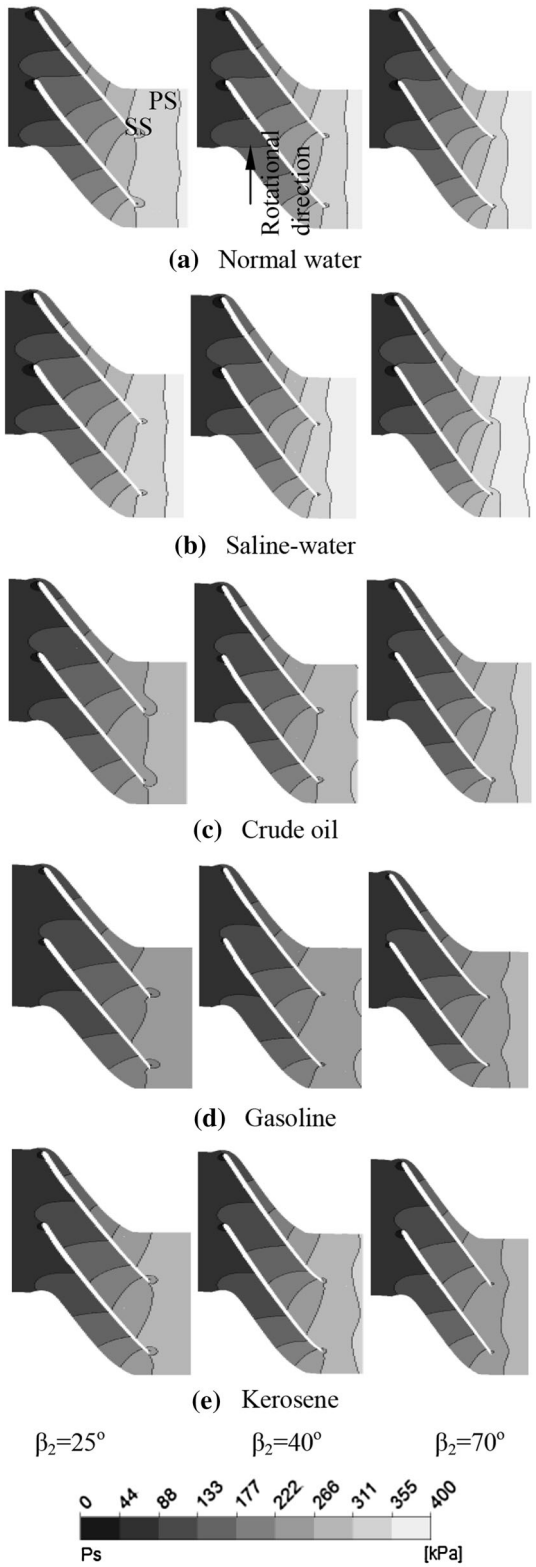

Fig. 6 Static pressure contours at 50 % ($Q = 0.1003$ m^3/s)

losses. Hence a moderate fall in efficiency is accounted. The combined effect of increase in β_2 and k_s values, the efficiency gets affected. Because of increase in surface

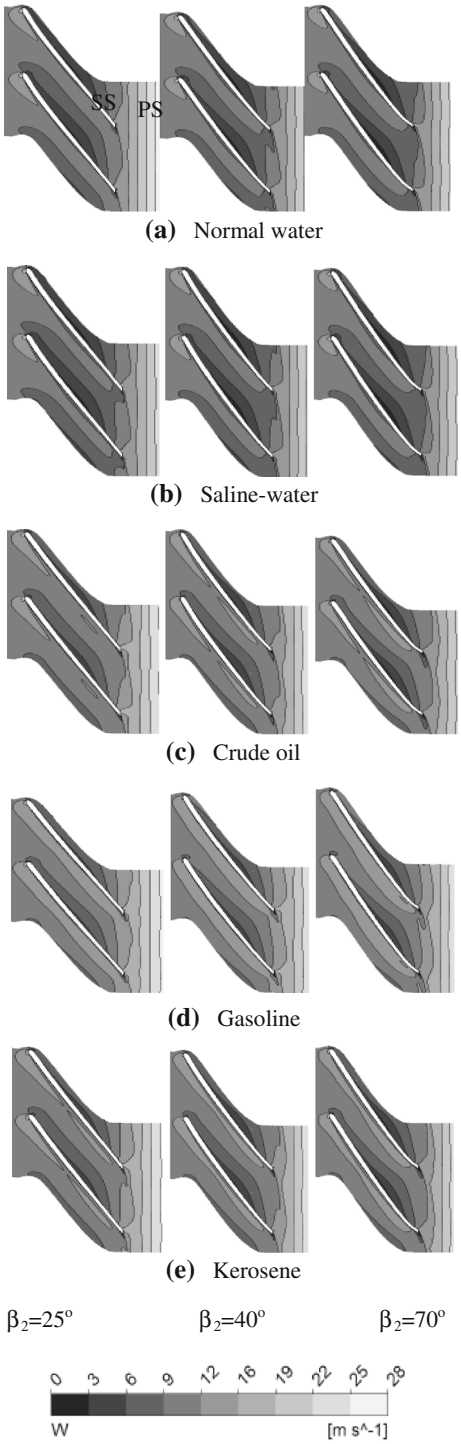

Fig. 7 Flow velocity contours at 50 % span ($Q = 0.1003$ m^3/s)

roughness, the head loss (ΔH) is more due to the secondary losses, profile losses and shock losses (Srinivasan 2008) (Eq. 11). Equation 15 illustrates that the surface roughness affects the friction and hence the impeller performance drops. In addition, the decrease in efficiency to pump crude oil and saline-water is due to the disc friction losses over the

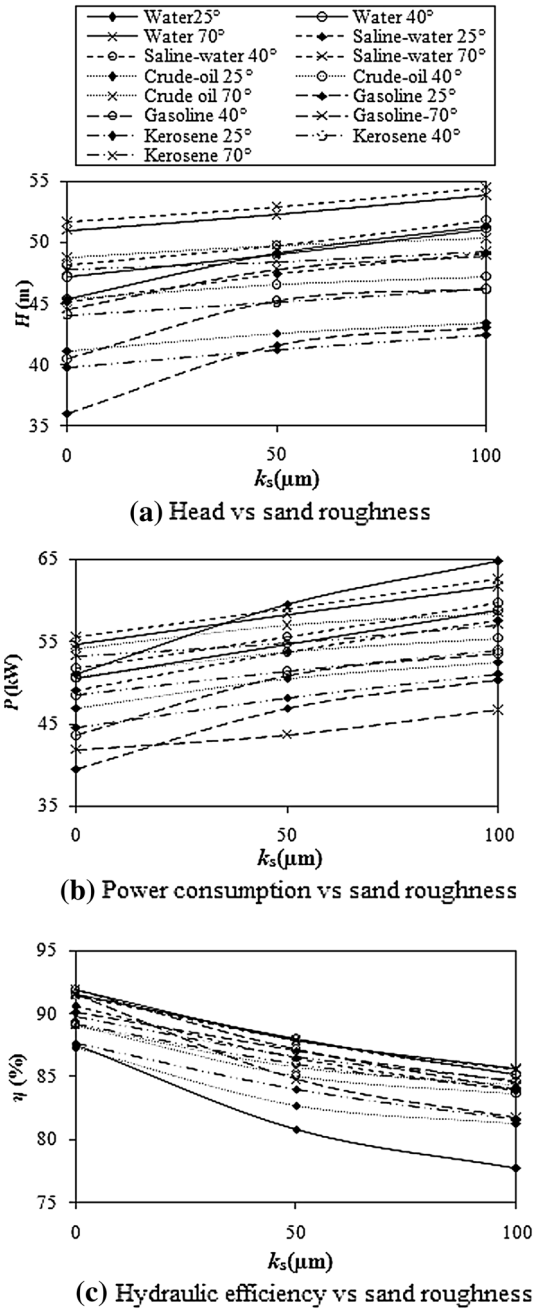

Fig. 8 Effect of surface roughness ($Q = 0.1003\ m^3/s$)

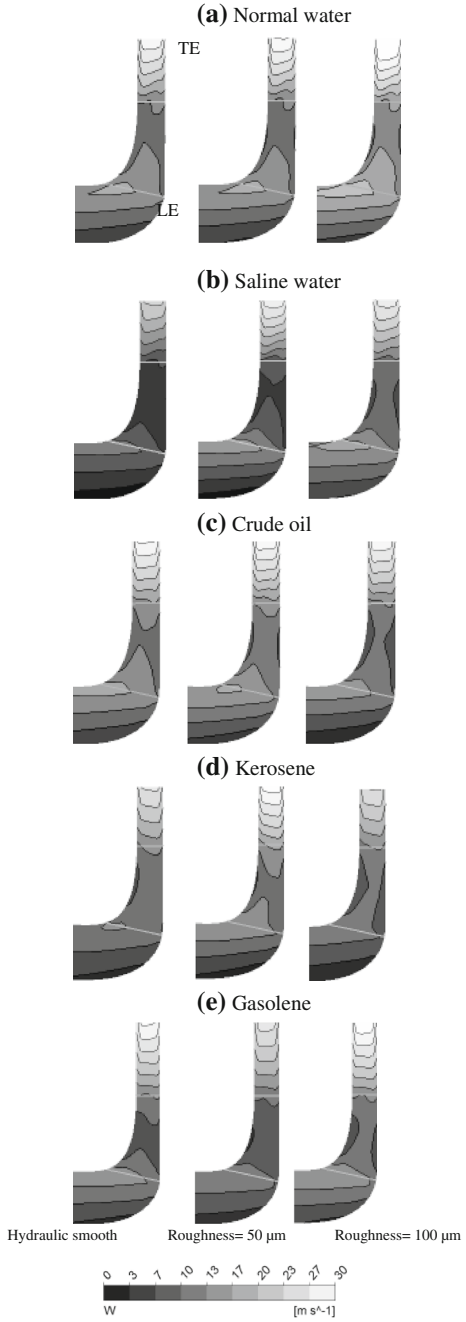

Fig. 9 Meridional velocity contours for different fluids at design point

outsides of the impeller shroud and hub. These results show a good agreement with the existing analytical results (Gulich 2010; Zhang 2011).

In a total combined increase in β_2 and k_s values increases the head and this leads to an increase in input power with a moderate fall in efficiency.

Hence, it is recommended that in case of crude oil pumping if the priority is to transport oil to a greater height, high surface roughness value and large exit angle can be introduced with a little compromise in efficiency. In other scenarios, if power saving and a fair overall pumping performance is a criterion, it is advised to select a moderate roughness value and exit blade angle.

Conclusions

Effects of exit blade angle and surface roughness on the centrifugal pump impeller performance at different mass flow rates have been evaluated by numerical simulations

for water, crude oil, saline-water gasoline and kerosene. The conclusions are:

- The blade exit angle has higher influence on the head, shaft power and hydraulic efficiency while the inlet blade angle has lower effect on the parameters. Large exit blade angle always augments head generation with increased input power consumption. Increase in exit blade angle increases the hydraulic efficiency till the design point. At off-design points, the efficiency decreases for higher exit blade angles because of different losses.
- Higher viscosity liquids have lower head generation at the same exit blade angle. An increase in fluid density results in increased power consumption at various blade exit angles.
- The efficiency drops with increase in surface roughness due to surface roughness effect, flow losses and external disc friction. Higher surface roughness helps getting higher head.
- Combined effect of increase in exit blade angle and surface roughness shows an in increase in head with negligible increase in efficiency.
- In crude oil industry, for high head oil transportation and more production, increase in surface roughness value with large exit blade angle is effective. Hence, prior to application, the design may consider design itself if there is possibility of surface deterioration with course of time. This will help reducing the total energy consumption.
- From energy saving point of view and a fair overall crude oil pumping performance, a moderate selection in surface roughness value and exit blade angle is suggested, and this can be implemented while designing the component.

Acknowledgments The authors would like to acknowledge Indian Institute of Technology Madras for the NFSC grant (Grant code: OEC/10-11/529/NFSC/ABDU) to conduct this research.

References

Ansys-CFX 13.0 (2010) Reference Guide, Ansys Inc

Aoki K, Ohta H, Nakayama Y (1987) Study on centrifugal pump for high viscosity liquids (The 1st Report, Effect of impeller output angle and number of blades on the pump performance of closed type impellers). Proceedings of the School of Engineering, Tokai university 27(2):151–158

Bayly BJ, Orszag SA (1988) Instability mechanisms in shear flow transition. Annu Rev Fluid Mech 20(1):359–391

Bellary SAI, Samad A (2014) An alternative approach to surrogate averaging for a centrifugal impeller shape optimisation. Computer Aided Engineering and Technology (Accepted for publication), Int. J

Bellary SAI, Husain A, Samad A (2014) Effectiveness of meta-models for multi-objective optimization of centrifugal impeller. J Mech Sci Technol 28(12):4947–4957

Church AH (1972) Centrifugal pump and blowers. 1st edn, John Wiley and sons, Inc., New York

Dean RC Jr., Senoo Y (1960) Rotating wakes in vaneless diffusers. ASME Journal of Basic Engineering September, pp 563–574

Desai J, Chauhan V, Charnia S, Patel K (2011) Validation of hydraulic design of a metallic volute centrifugal pump using CFD. The 11th Asian International Conference on Fluid Machinery and 3rd Fluid Power Technology Exhibition, 21–23 Nov., IIT Madras, Chennai

Fard MHS, Boyaghchi FA (2007) Studies on the influence of various blade outlet angles in a centrifugal pump when handling viscous fluids. Am J Appl Sci 4(9):718–724

Fard MHS, Tahani M, Ehghaghi MB, Fallahian MA, Beglari M (2012) Numerical study of the effects of some geometric characteristics of a centrifugal pump impeller that pumps a viscous fluid. Comput Fluids 60:61–70

Gulich JF (2010) Centrifugal Pumps. Springer Publications, 2nd edn, Berlin

Ippen AT (1946) The influence of viscosity on centrifugal performance. Trans ASME 68(8):823–830

Itaya S, Nishikawa T (1960) Studies on the volute pumps handling viscous fluids. Bull JSME 26(162):202–212

Johnston JP, Rothe PH (1967) Effect of system rotation on the performance of two-dimensional diffusers. ASME J Fluids Eng, pp 422–430

Johnston PJ, Halleen RM, Lezius DK (1972) Effects of spanwise rotation on the structure of two-dimensional fully developed channel flow. J Fluid Mech 56(3):533–557

Kamimoto G, Matsuoka Y (1956) On the flow in the impeller of centrifugal type hydraulic machinery (The 2nd report). Trans JSME Series 3, 22(113):55–59

Lazarkiewicz S, Troskolanski AT (1965) Impeller pumps. 1st edn, Pergamon Press Ltd., Oxford

Li WG (2008) Numerical study on behavior of a centrifugal pump when delivering viscous oils-part1: performance. Int J Turbo Jet Engines 25:61–79

Li WG (2011a) Blade exit angle effects on performance of a standard industrial centrifugal oil pump. J Appl Fluid Mech 4(2):105–119

Li WG (2011b) Effect of exit blade angle, viscosity and roughness in centrifugal pumps investigated by cfd computations. Task Quarterly 15(1):21–41

Luo X, Zhang Y, Peng L, Xu H, Yu W (2008) Impeller inlet geometry effect on performance improvement for centrifugal pumps. J Mech Sci Technol 22:1971–1976

Murakami M, Kikuyama K, Asakura E (1980) Velocity and pressure distributions in the impeller passages of centrifugal pump. ASME J. Fluids Eng 102:420–426

Ohta H, Aoki K (1996) Effect of impeller angle on performance and internal flow of centrifugal pump for high viscosity liquids. Proc School Eng Tokai Univ 36(1):159–168

Samad A, Kim KY (2008) Shape optimization of an axial compressor blade by multi-objective genetic algorithm. Proc. IMechE Part A. J. Power Energy 222:599–611

Sanda B, Daniela CV (2012) The influence of the inlet angle over the radial impeller geometry design approach with Ansys. J Eng Studies Res 18(4):32–39

Shigemitsu T, Fukutomi J, Nasada R, Kaji K (2011) The effect of blade outlet angle on performance and internal flow condition of mini turbo-pump. J Therm Sci 20(1):32–38

Srinivasan KM (2008) Rotodynamic pumps. New Age International (P) Ltd., New Delhi

Stepanoff AJ (1940) Pumping viscous oils with centrifugal pumps. Oil Gas J 1(4)

Stepanoff AJ (1964) Centrifugal and axial flow pumps. 2nd edn, John Wiley and Sons inc., New York

Telow N (1942) A survey of modern centrifugal pump practice for oilfield and Oil Refinery Services. The Institution of Mechanical Engineering 3(121)

Tuzson J (1993) Interpretation of impeller flow calculations. ASME J Fluid Eng, pp 463–467

Tuzson J (2000) Centrifugal pump design. 1st edn, John Wiley and Sons, Inc., New York

Varley FA (1961) Effects of impeller design and surface roughness on the performance of centrifugal pumps. Proc Instn Mech Eng 175(21):955–969

Wilcox DC (1994) Turbulence modeling for CFD. 2nd edn, DCW Industries, Inc., La Canada, California

Zhang Y, Zhou X, Ji Z, Jiang C (2011) Numerical design and performance prediction of low specific speed centrifugal pump impeller. Int J Fluid Machin Syst 4(1):133–139